On Performance of Nine-Node Quadrilateral Shell Elements 9-EAS11 and MITC9i

K. Wiśniewski and E. Turska

Abstract The chapter concerns nine-node quadrilateral shell elements derived for the Reissner-Mindlin kinematics and Green strain. They are based on the potential energy functional extended to include drilling rotations. A standard element of this class suffers from locking and over-stiffening; several special techniques are needed to improve its performance. We developed three nine-node shell elements with the membrane strains enhanced by the EAS11 representation of Bischoff and Ramm (Int. J. Num. Meth. Eng. 40:4427–4449, 1997 [2]). The transverse shear strains are treated either by the ANS method of Jang and Pinsky (Int. J. Num. Meth. Eng. 24:2389–2411, 1987 [6]), or are enhanced by the EAS6 representation of Sansour and Kollmann (Comput. Mech. 24:435–447, 2000 [17]), or remain unmodified. We also modify the EAS transformation rule, extending the idea put forward in Park and Lee (Comput. Mech. 15:473–484, 1995 [15]) for curved shells. Several numerical examples provide comparison of three 9-EAS11 elements to our MITC9i shell element of Wisniewski and Turska (Comput. Mech. 62, 499–523, 2018 [20]).

1 Introduction

The chapter concerns nine-node quadrilateral shell elements derived for the Reissner-Mindlin kinematics and Green strain. They are based on the potential energy functional extended to include the drilling rotation. The standard element of this class suffers from locking and over-stiffening, and several special techniques are needed to improve its performance. Our best MITC9i shell element described in [20] is based on the method of *improved two-level approximations* of covariant strains (MITCi),

K. Wiśniewski (✉)

Institute of Fundamental Technological Research, Polish Academy of Sciences, Warsaw, Poland
e-mail: kwisn@ippt.pan.pl

E. Turska

Polish Japanese Academy of Information Technology, Warsaw, Poland
e-mail: eturska@pjwstk.edu.pl

and was gradually developed in [13, 14, 21]. The other important features of this element are as follows:

1. To reduce shape distortion effects, the so-called Corrected Shape Functions (CSF) of [3] are extended to shells and used instead of the standard ones. In effect, all patch tests are also passed for shifts of the midside nodes along straight element sides and for arbitrary shifts of the central node.
2. Several extensions of the CSF are proposed to enable computations of non-flat shells. In particular, a criterion is put forward to determine the shift parameters associated with the central node for non-flat elements. Additionally, a method is presented to construct a parabolic side for a shifted midside node, which improves accuracy for symmetric curved edges.
3. Drilling rotations are included by using the drilling Rotation Constraint equation, in a way consistent with the additive/multiplicative rotation update scheme for large rotations. It is shown that the CSF reduce the sensitivity of a solution to the regularization parameter γ of the penalty method for this constraint.

In the current chapter, we compare the MITC9i shell element to the nine-node shell elements with the membrane strains enhanced by the EAS11 representation of [2]. The transverse shear strains are treated either by the ANS method of [6], or are enhanced by the EAS6 representation of [17], or remain unmodified. We also modify the EAS transformation rule extending the idea put forward in [15]. Several numerical examples provide comparison of three 9-EAS11 elements to our MITC9i shell element.

## 2   Basic Shell Equations with Drilling Rotation

Two-field functional In the present work, we use a two-field extended shell functional depending on displacements and three-parameter rotations,

$$F_2(\boldsymbol{\chi}, \mathbf{Q}_0) \doteq \int_B \mathscr{W}(\mathbf{C}) \, \mathrm{d}V + F_{\text{ext}} + F_{\text{drill}}(\boldsymbol{\chi}, \mathbf{Q}_0), \qquad (1)$$

where $\boldsymbol{\chi}$ is the deformation function and $\mathbf{Q}_0 \in SO(3)$ is the rotation tensor. The strain energy density $\mathscr{W}$ depends on the right Cauchy-Green deformation tensor $\mathbf{C} \doteq \mathbf{F}^T \mathbf{F}$, where $\mathbf{F} \doteq \nabla \boldsymbol{\chi}$ is the deformation gradient. F_{ext} is the potential of external loads. The last component in Eq. (1) is added to incorporate the drilling rotation using the penalty method,

$$F_{\text{drill}} \doteq \frac{1}{2} \int_M \gamma \, c^2 \, \mathrm{d}A, \qquad c \doteq \frac{1}{2} \left[(\mathbf{F}_0 \mathbf{t}_2) \cdot (\mathbf{Q}_0 \mathbf{t}_1) - (\mathbf{F}_0 \mathbf{t}_1) \cdot (\mathbf{Q}_0 \mathbf{t}_2) \right], \qquad (2)$$

Fig. 1 The reference surface ($\zeta = 0$) of nine-node shell element
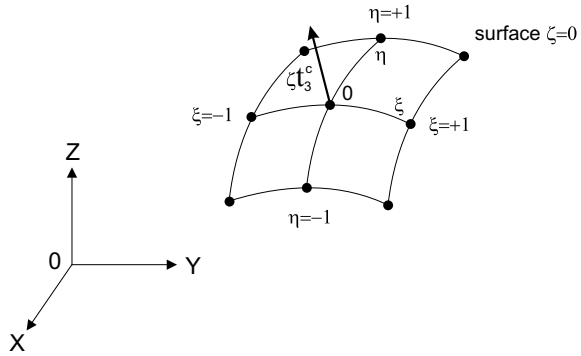
where c is the l.h.s. of the $(1, 2)$ component of the Rotation Constraint (RC) equation, $\text{skew}(\mathbf{Q}_0^T \mathbf{F}_0) = \mathbf{0}$, and $\gamma \in (0, \infty)$ is the regularization parameter; the importance of this constraint was already noticed in [1] though it was used for a different purpose. Note that $\mathbf{F}_0$ and $\mathbf{Q}_0$ are associated with the reference (middle) shell surface for the initial configuration, and $\mathbf{t}_1$ and $\mathbf{t}_2$ are the tangent vectors of the local Cartesian basis on this surface.

Reissner-Mindlin kinematics The initial configuration of the shell is parameterized by the natural coordinates $\xi, \eta \in [-1, +1]$ on the reference (middle) surface, and the normal coordinate $\zeta \in [-h/2, +h/2]$, where h is the initial shell thickness, see Fig. 1. For the deformed configuration, we use the Reissner-Mindlin kinematical assumptions,

$$\mathbf{x}(\xi, \eta, \zeta) = \mathbf{x}_0(\xi, \eta) + \zeta \, \mathbf{Q}_0(\xi, \eta) \, \mathbf{t}_3(\xi, \eta), \tag{3}$$

where $\mathbf{x}$ is a position vector at an arbitrary ζ and $\mathbf{x}_0$ at $\zeta = 0$. Besides, $\mathbf{t}_3$ is the unit normal vector in the initial configuration. The rotation tensor $\mathbf{Q}_0$ is parameterized by the canonical rotation vector $\boldsymbol{\psi}$,

$$\mathbf{Q}_0(\boldsymbol{\psi}) \doteq \mathbf{I} + \frac{\sin \omega}{\omega} \tilde{\boldsymbol{\psi}} + \frac{1 - \cos \omega}{\omega^2} \tilde{\boldsymbol{\psi}}^2, \tag{4}$$

where $\omega = \|\boldsymbol{\psi}\| = \sqrt{\boldsymbol{\psi} \cdot \boldsymbol{\psi}} \geq 0$ and $\tilde{\boldsymbol{\psi}} \doteq \boldsymbol{\psi} \times \mathbf{I}$. This parametrization is used within the load step, and is a part of the rotation update scheme based on quaternions, to handle unrestricted rotations.

The deformation function $\boldsymbol{\chi} : \mathbf{x} = \boldsymbol{\chi}(\mathbf{X})$ maps the initial (non-deformed) configuration of a shell onto the current (deformed) one. Let us write the deformation gradient as follows:

$$\mathbf{F} \doteq \frac{\partial \mathbf{x}}{\partial \mathbf{X}} = \frac{\partial \mathbf{x}}{\partial \boldsymbol{\xi}} \, \mathbf{J}^{-1}, \tag{5}$$

where $\boldsymbol{\xi} \doteq \{\xi, \eta, \zeta\}$ and the Jacobian matrix $\mathbf{J} \doteq \partial \mathbf{X}/\partial \boldsymbol{\xi}$. The right Cauchy-Green deformation tensor is $\mathbf{C} \doteq \mathbf{F}^T \mathbf{F}$ and the Green strain is defined as $\mathbf{E} \doteq \dfrac{1}{2}(\mathbf{C} - \mathbf{C}_0)$, where $\mathbf{C}_0 \doteq \mathbf{C}|_{\mathbf{x}=\mathbf{X}} = \mathbf{I}$. The Green strain can be linearized in ζ,

$$\mathbf{E}(\zeta) \approx \mathbf{E}_0 + \zeta \mathbf{E}_1, \tag{6}$$

where the *0th order* strain $\mathbf{E}_0$ includes the membrane components $\boldsymbol{\varepsilon}$ and the transverse shear components $\boldsymbol{\gamma}/2$ while the *1st order* strain $\mathbf{E}_1$ includes the bending/twisting components $\boldsymbol{\kappa}$. The transverse shear part of $\mathbf{E}_1$ is typically neglected, i.e. $\kappa_{\alpha 3} \approx 0$ ($\alpha = 1, 2$). By Eq. (3), the normal strains ε_{33} and κ_{33} are equal to zero and must be either recovered from an auxiliary condition, such as the plane stress condition used in the current chapter, or be introduced by the EAS method.

3 Corrected Shape Functions for Nine-Node Shell Element

The standard isoparametric shape functions for a nine-node element are derived assuming that the midside nodes (5, 6, 7, 8) are located at the middle positions between the corner nodes, and that the central node 9 is located at the element center, see Fig. 2a. When these nodes are shifted from the middle positions then the physical space parameterized by the standard shape functions is distorted, see e.g. Figs. 13a and 20 in [14].

To alleviate this problem, in [3] the Corrected Shape Functions (CSF) were proposed with six additional parameters $\alpha, \beta, \gamma, \varepsilon, \theta, \kappa \in [-1, +1]$, see Fig. 2b, which define shifts of the midside nodes and the central node from the middle positions in the local coordinates space. The CSF for the nine-node element are defined in two steps. First, the CSF of the eight-node (serendipity) element are defined,
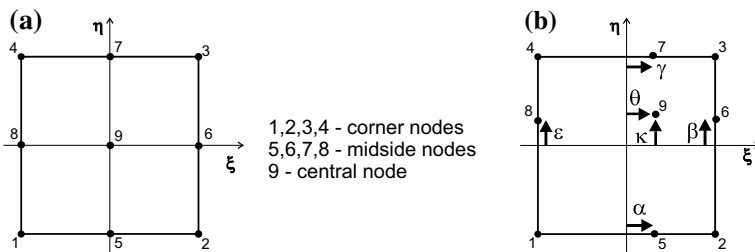

Fig. 2 Nine-node element: **a** Numbering and naming of nodes, **b** Shift parameters

$$\bar{N}_1 \doteq \frac{1}{4}(1-\xi)(1-\eta)\frac{(1+\alpha)(1+\varepsilon)-(1+\alpha)(1+\eta)-(1+\varepsilon)(1+\xi)}{(1+\alpha)(1+\varepsilon)},$$

$$\bar{N}_2 \doteq \frac{1}{4}(1+\xi)(1-\eta)\frac{(1-\alpha)(1+\beta)-(1-\alpha)(1+\eta)-(1+\beta)(1-\xi)}{(1-\alpha)(1+\beta)},$$

$$\bar{N}_3 \doteq \frac{1}{4}(1+\xi)(1+\eta)\frac{(1-\gamma)(1-\beta)-(1-\gamma)(1-\eta)-(1-\beta)(1-\xi)}{(1-\gamma)(1-\beta)},$$

$$\bar{N}_4 \doteq \frac{1}{4}(1-\xi)(1+\eta)\frac{(1+\gamma)(1-\varepsilon)-(1+\gamma)(1-\eta)-(1-\varepsilon)(1+\xi)}{(1+\gamma)(1-\varepsilon)}, \qquad (7)$$

$$\bar{N}_5 \doteq \frac{(\xi^2-1)(1-\eta)}{2(\alpha^2-1)}, \qquad \bar{N}_6 \doteq \frac{(1+\xi)(\eta^2-1)}{2(\beta^2-1)},$$

$$\bar{N}_7 \doteq \frac{(\xi^2-1)(1+\eta)}{2(\gamma^2-1)}, \qquad \bar{N}_8 \doteq \frac{(1-\xi)(\eta^2-1)}{2(\varepsilon^2-1)},$$

which account for shifts of the midside nodes from the middle positions. Next, the basis function for the central node 9 is added hierarchically to them. The obtained CSF for the nine-node element are as follows:

$$N_i(\xi, \eta) = \bar{N}_i(\xi, \eta) - \bar{N}_i(\theta, \kappa)\, N_9(\xi, \eta), \qquad i = 1, \ldots, 8,$$

$$N_9 \doteq \frac{(\xi^2-1)(\eta^2-1)}{(\theta^2-1)(\kappa^2-1)}, \qquad (8)$$

where $\bar{N}_i(\theta, \kappa) \doteq \bar{N}_i(\xi = \theta, \eta = \kappa)$, see [3], Eq. (20). When the shift parameters are equal to zero, then the CSF of Eq. (8) reduce to the standard shape functions.

These six parameters are computed as proportional to the distance in the physical space, and to determine them, several nonlinear equations must be solved: 4 equations with 1 unknown for the midside nodes and 2 equations with 2 unknowns for the central node. This is done only once, so the time overhead is insignificant.

In [20], several extensions of the method of calculating the shift parameters are presented, which enable the use of the CSF for nine-node shell elements located in 3D space. They provide an improved accuracy of a solution for non-flat shell elements. Besides a method of constructing symmetric side curves for shifted midside nodes is described; we refer a reader interested in details to this paper. The so-extended CSF can also be applied to the 9-EAS11 shell elements, and, as our tests prove, they can be very beneficial, e.g. they are needed to pass the bending patch test for some types of nodal shifts.

4 Characteristics of 9-EAS11 Shell Elements

In the current chapter, we consider the class of nine-node shell elements with the *Enhanced Assumed Strain* (EAS) method applied to membrane strains. The EAS method was introduced in [18] for four-node elements; in this method, the compatible

strains $\mathbf{E}^c$ are enhanced additively, i.e. $\mathbf{E} = \mathbf{E}^c + \mathbf{E}^{enh}$, where $\mathbf{E}^{enh}$ is obtained from covariant components in a basis at the element center ("c").

Enhancement of membrane strains The EAS enhancement of the membrane strains $\boldsymbol{\varepsilon}$ is constructed at a Gauss Point "g" as follows:

$$\mathbf{E}_g^{enh} = \mathbf{J}_c^{-T} \, \mathbf{E}_{\xi g} \, \mathbf{J}_c^{-1} \left(\frac{j_c}{j_g} \right), \qquad \mathbf{E}_\xi \doteq \begin{bmatrix} E_{11} & E_{12} & 0 \\ E_{12} & E_{22} & 0 \\ 0 & 0 & 0 \end{bmatrix}, \qquad (9)$$

where the Jacobian is $\mathbf{J}_c \doteq [\ \mathbf{g}_1^c \ | \ \mathbf{g}_2^c \ | \ \frac{h}{2}\mathbf{t}_3^c \ ]$ and $\mathbf{g}_1^c, \mathbf{g}_2^c$ are natural vectors at the element center. Note that a general rule to transform the covariant components $\mathbf{E}_\xi$ to the Cartesian ones is $\mathbf{E}^{CART} = \mathbf{J}^{-T} \, \mathbf{E}_\xi \, \mathbf{J}^{-1}$, see [19] Eq. (2.24) or [22] Eq. (7).

In the 9-EAS11 shell elements, the membrane strains $\boldsymbol{\varepsilon}$ are enhanced by the representation with 11 multipliers q_i, as in [2] Eq. (30),

$$\begin{aligned} E_{11} &= P_\xi \, (q_1 + \eta q_2 + \eta^2 q_3), \\ E_{22} &= P_\eta \, (q_9 + \xi q_{10} + \xi^2 q_{11}), \\ E_{12} &= P_\xi (q_4 + \eta q_5) + P_\eta (q_6 + \xi q_7) + P_\xi P_\eta q_8, \end{aligned} \qquad (10)$$

where $P_\xi \doteq 1 - 3\xi^2$ and $P_\eta \doteq 1 - 3\eta^2$. This representation uses the following polynomial bases:

$$\begin{aligned} E_{11} &: \ \{P_\xi, \ P_\xi \eta, \ P_\xi \eta^2\}, \\ E_{22} &: \ \{P_\eta, \ P_\eta \xi, \ P_\eta \xi^2\}, \\ E_{12} &: \ \{P_\xi, \ P_\eta, \ P_\xi \eta, \ P_\eta \xi, \ P_\xi P_\eta\}. \end{aligned} \qquad (11)$$

We applied to each of these bases, the Gram-Schmidt orthogonalization with respect to the inner product function $\int_{-1}^{+1} \int_{-1}^{+1} f_i f_k \, \mathrm{d}\xi \mathrm{d}\eta$, where f_i, f_k are terms of the basis considered, and obtained

$$\begin{aligned} E_{11} &: \ \{A \, P_\xi, \ B \, P_\xi \eta, \ -C \, P_\xi \eta^2\}, \\ E_{22} &: \ \{A \, P_\eta, \ B \, P_\eta \xi, \ -C \, P_\eta \xi^2\}, \\ E_{12} &: \ \{A \, P_\xi, \ A \, P_\eta, \ B \, P_\xi \eta, \ B \, P_\eta \xi, \ C \, P_\xi P_\eta\}, \end{aligned} \qquad (12)$$

where $A \doteq \sqrt{5}/4$, $B \doteq \sqrt{15}/4$ and $C \doteq 5/8$. Hence, the bases of Eq. (11) are orthogonal and this procedure only renormalized them. When the bases of Eq. (12) are used in Eq. (10), then A, B and C only affect values of multipliers q_i. We have checked on the example of Sect. 5.3 that the use of Eq. (12) does not change the solution indeed.

The EAS transformation rule for curved shells A Jacobian at the element center is used in Eq. (9), hence, this transformation can be inadequate for curved shells. To account for a shell curvature but to retain the original form of Eq. (9) for flat shells,

we modified the idea of [15], which uses at Gauss points, the Cartesian basis for the element center properly rotated forward; it is designated *Local coordinate system 2*, see p. 478 therein. Because we need to determine the Jacobian $\mathbf{J} \doteq [\, \mathbf{g}_1 \mid \mathbf{g}_2 \mid \frac{h}{2} \mathbf{t}_3 \,]$ at a Gauss point, we apply this idea to the vectors $\mathbf{g}_1$ and $\mathbf{g}_2$ as follows:

1. The normal vectors, $\mathbf{t}_3^c$ at the element center and $\mathbf{t}_3^g$ at a Gauss point, are computed in a standard manner.
2. $\mathbf{t}_3^c$ is rotated into $\mathbf{t}_3^g$ by the canonical rotation vector $\mathbf{v} \doteq \theta \mathbf{n}$, where

$$\mathbf{n} = \mathbf{t}_3^c \times \mathbf{t}_3^g / \|\mathbf{t}_3^c \times \mathbf{t}_3^g\|, \qquad \theta \doteq \arccos(\mathbf{t}_3^c \cdot \mathbf{t}_3^g). \tag{13}$$

Here the vector $\mathbf{n}$ defines an axis of rotation and θ is the rotation angle. A corresponding rotation tensor $\mathbf{R}(\mathbf{v})$ is defined by Eq. (4), where $\boldsymbol{\psi}$ is replaced by $\mathbf{v}$. Note that $\mathbf{t}_3^g = \mathbf{R}(\mathbf{v})\, \mathbf{t}_3^c$ by definition.

3. The natural basis vectors at the element center are forward-rotated to the Gauss point as follows:

$$\mathbf{g}_1^* = \mathbf{R}(\mathbf{v})\, \mathbf{g}_1^c, \qquad \mathbf{g}_2^* = \mathbf{R}(\mathbf{v})\, \mathbf{g}_2^c. \tag{14}$$

Alternatively, we can re-write Eq. (14) using Eq. (8.6) of [19] as follows:

$$\begin{aligned} \mathbf{g}_1^* &= \mathbf{g}_1^c + s\,(\mathbf{n} \times \mathbf{g}_1^c) + (1-c)[\mathbf{n} \times (\mathbf{n} \times \mathbf{g}_1^c)], \\ \mathbf{g}_2^* &= \mathbf{g}_2^c + s\,(\mathbf{n} \times \mathbf{g}_2^c) + (1-c)[\mathbf{n} \times (\mathbf{n} \times \mathbf{g}_2^c)], \end{aligned} \tag{15}$$

where $c \doteq \cos\theta = \mathbf{t}_3^c \cdot \mathbf{t}_3^g$ and $s \doteq \sin\theta = \sin(\arccos(c))$. Note that these formulas are different than those of [15] Eq. (31).

4. Using Eq. (14) or (15), we can define the modified Jacobian $\mathbf{J}^* \doteq [\, \mathbf{g}_1^* \mid \mathbf{g}_2^* \mid \frac{h}{2} \mathbf{t}_3^g \,]$. Note that $\mathbf{J}^* = \mathbf{R}(\mathbf{v})\, \mathbf{J}_c$, and we can use its inverse $(\mathbf{J}^*)^{-1} = \mathbf{J}_c^{-1} \mathbf{R}^T(\mathbf{v})$ instead of $\mathbf{J}_c^{-1}$ in Eq. (9). For flat shells, $\mathbf{v} = \mathbf{0}$, hence, $\mathbf{R}(\mathbf{v}) = \mathbf{I}$ and $(\mathbf{J}^*)^{-1} = \mathbf{J}_c^{-1}$, as required.

Remark. The forward-rotated Cartesian basis of [15] was proposed to obtain invariant *Assumed Strain* elements, which can pass both the patch and locking tests. (The *Assumed Strain* method in this paper does not use the *two-level interpolations* of strains; hence, it is different than a method of the same name of [4]). The independent strain fields are assumed with respect to a local coordinate system defined at the element centroid, e.g. for the shell with six degrees of freedom per node, 52 terms are assumed. The numerical results of [15] indicate that their elements perform well, but effects of the new *Local coordinate system 2* on accuracy for curved shells and distorted meshes are mixed; e.g. in the "Pinched ring" example accuracy worsens.

The modified EAS transformation rule for curved shells of Eq. (14) was implemented in our 9-EAS11 shell elements and tested in Sect. 5.2; no improved accuracy was obtained in this test, but, undoubtedly, more tests are necessary to draw a final conclusion.
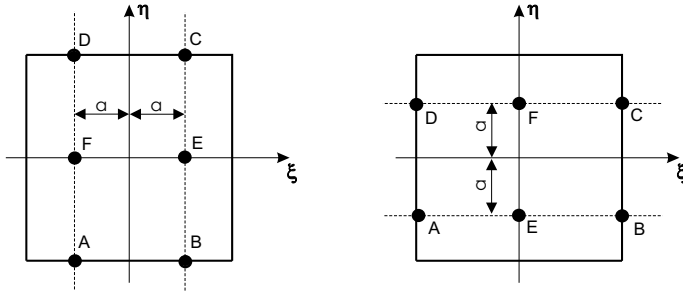
Fig. 3 Sampling points used in [6] for: **a** γ_{31} and **b** γ_{32}. $a = \sqrt{1/3}$

Treatment of transverse shear strains The transverse shear strains γ are treated in the 9-EAS11 shell elements in three ways:

1. By using the ANS of [6], where the two-level approximations are applied to the covariant (COV) components, which involves the 2×3 and 3×2 tying point schemes of Fig. 3 and the following interpolation functions:

$$\gamma_{31}: \qquad \bar{N}_1 = \frac{\eta(\eta - 1)}{2}, \quad \bar{N}_2 = 1 - \eta^2, \quad \bar{N}_3 = \frac{\eta(\eta + 1)}{2}, \qquad (16)$$

$$\gamma_{32}: \qquad \bar{S}_1 = \frac{\xi(\xi - 1)}{2}, \quad \bar{S}_2 = 1 - \xi^2, \quad \bar{S}_3 = \frac{\xi(\xi + 1)}{2}. \qquad (17)$$

The same locations of the tying points were used earlier in [5].

2. By using the EAS method, with the transformation rule of Eq. (9) and the matrix

$$\mathbf{E}_\xi \doteq \begin{bmatrix} 0 & 0 & E_{13} \\ 0 & 0 & E_{23} \\ E_{13} & E_{23} & 0 \end{bmatrix}. \qquad (18)$$

The covariant transverse shear components of the enhancement are assumed as in [17], Eqs. (127) and (128),

$$E_{13} = P_\xi \, (q_1 + \eta q_2 + \eta^2 q_3), \qquad E_{23} = P_\eta \, (q_4 + \xi q_5 + \xi^2 q_6), \qquad (19)$$

where 6 parameters are used—this variant is designated EAS6.

3. By using unmodified transverse shear strains.

Finally, the bending/twisting strain κ is unmodified in the tested 9-EAS11 elements.

Table 1 Tested 9-EAS11 shell elements with drilling rotation

Element	CSF	Strains		
		Membrane ε	Bending κ	Transverse shear γ
Tested elements				
9-EAS11/DISP/ANS [2]	No	EAS11	DISP	ANS of [6]
9-EAS11/DISP/EAS6 [17]	No	EAS11	DISP	EAS6 of [17], Eqs. (127) and (128)
9-EAS11/DISP/DISP [own]	No	EAS11	DISP	DISP
Reference element				
MITC9i [20]	Yes	MITCi	MITCi	MITCi
16-DISP, 4×4 GP [own]	No	DISP	DISP	DISP

5 Numerical Examples

In this section, we present numerical tests of three nine-node 9-EAS11 shell elements described in Sect. 4 and listed in Table 1, where "DISP" means that the strain is not modified.

All the tested and reference shell elements are of the Reissner-Mindlin type and have 6 dofs/node; the drilling rotation is incorporated as specified in Eqs. (1) and (2), for more details see Sects. 2 and 5 of [20]. Note that in all these elements:

1. the CSF are implemented in the version extended for shells of [20], Sect. 4, which enables calculation of shift parameters for non-flat elements.
2. the 3×3 Gauss integration is used in all nine-node elements, and they all have a correct rank.

All these FEs were derived by ourselves using the automatic differentiation program AceGen described in [8], and were tested within the finite element program FEAP developed by Taylor [23]. The use of these programs is gratefully acknowledged. Our parallel multithreaded (OMP) version of FEAP is described in [7].

5.1 Patch Tests

The standard five-element patch of elements was proposed in [16] and we run this test also for the mesh distorted by shifts of nodes shown in Fig. 4. The membrane and bending patch tests are performed as described in [12]; the transverse shear test is performed for the load case defined for a nine-node plate in [5], see "Shearing case" in Fig. 2b therein.

Four cases of nodal shifts are considered, see Fig. 4: (A) zero shifts (regular mesh), (B) arbitrary shifts of node 25, (C) parallel shifts of nodes 21–24, and (D)

Fig. 4 Five-element patch test for the mesh distorted by shifts of some nodes (circles not to scale)

perpendicular shifts nodes 21–24, for which edges of the central element are curved. For more details on these tests see [20]. The conclusions are as follows:

1. For the 9-EAS11 elements, the membrane patch test is passed for all cases of nodal shifts for the standard shape functions. As the CSF are not needed, we can say that 9-EAS11 performs better than MITC9i, which needs the CSF to pass Case B and C, and, even with the CSF, fails for Case D.
2. For the method 1 and 2 of treating the transverse shear described in Sect. 4, and for the standard shape functions (no CSF), the bending patch test is passed for Case A but is failed for Cases B, C and D.

   Therefore, we implemented the CSF also in the 9-EAS11 elements sand found that then they pass Case B and C but fail for Case D. The level of errors is similar to that for MITC9i. We see that the CSF are indispensable though they also do not solve the problem of curved edges (Case D).
3. The transverse shear patch test is passed for the standard shape functions (no CSF) for all cases of shifts.

5.2 Curved Cantilever

The curved cantilever is fixed at one end and loaded by a moment M_z at the other, see Fig. 5. The data is as follows: $E = 2 \times 10^5$, $\nu = 0$, width $b = 0.025$ and radius of curvature $R = 0.1$. The FE mesh consists of 6 nine-node elements, which have either regular (Fig. 5a) or distorted shape (Fig. 5b); a definition of distortions is given in [9] p. 245. For the distorted mesh, this test is very demanding.

The shell thickness h is varied in the range $[10^{-2}, 10^{-6}]$, and the moment is assumed as $M_z = (R/h)^{-3}$, so the solution of a linear problem should remain constant. The analytical solution for the curved beam subjected to uniform bending is $u_y = M_z R^2/(EI) = 0.024$, where I is the moment of inertia.
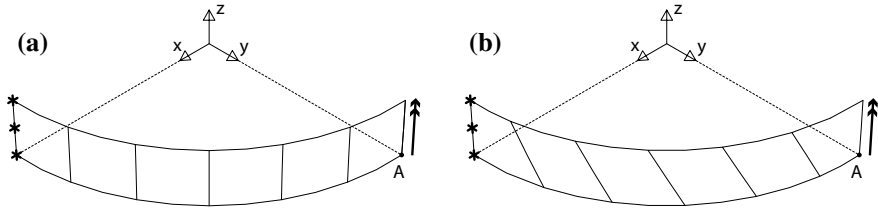
(a)

(b)

Fig. 5 Curved cantilever and two meshes: **a** regular and **b** distorted

(a)

displacement $-u_y$

MITC9i, regular mesh
9–EAS11/DISP/ANS
9–EAS11/DISP/EAS6
9–EAS11/DISP/DISP
MITC9i
MITC9i+RBF

slenderness R/h
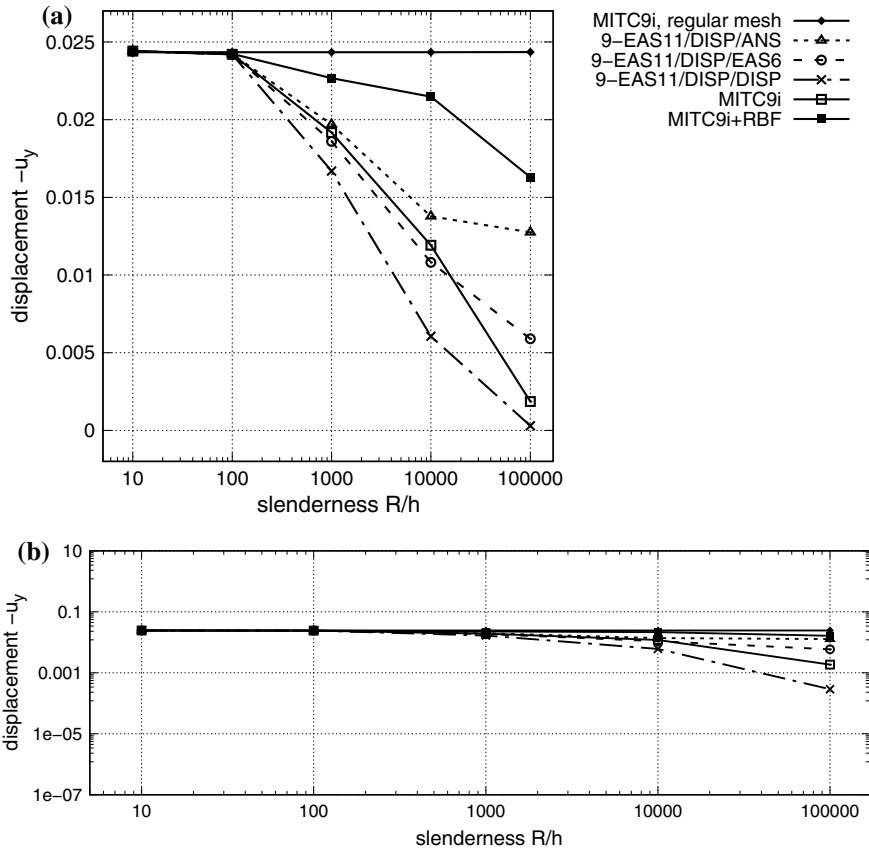
(b)

displacement $-u_y$

slenderness R/h

Fig. 6 Curved cantilever. Displacement u_y at point A for the distorted mesh and diminishing thickness. $\gamma = G$. **a** log-standard scale, **b** log-log scale to enable comparisons with Fig. 6 of [9]

The displacement u_y at point A obtained by a linear analysis are shown in Fig. 6, where, for the vertical axis, we use either (a) the standard scale or (b) the logscale, to enable comparisons with Fig. 6 of [9]. We conclude this test as follows:

1. For the regular mesh, the solutions for all tested elements are represented by the horizontal line, which is close to the analytical value. Neither one of the tested elements locks for this mesh despite its curvature. The basic element '9-DISP' severely locks for this mesh; this solution is not shown in these figures.
2. For the distorted mesh, all the tested elements lock for the $R/h > 100$. The most accurate is 9-EAS11/DISP/ANS, then MITC9i, 9-EAS11/DISP/EAS6 and 9-EAS11/DISP/DISP. The CSF are not important for this test.

We performed several additional tests to shed some light on the locking for the distorted mesh, and we found that:

1. The 9-URI2×2 element does not lock for the distorted mesh; this curve is not shown in Fig. 6. (It is the nine-node Uniformly Reduced Integration (2×2 Gauss points) element, which has 7 spurious zero eigenvalues).
2. The Residual Bending Flexibility (RBF) correction, which is a means to handle the sinusoidal bending and an extreme slenderness, significantly improves the results of this test; compare curves for MITC9i and MITC9i+RBF in Fig. 6.

For the nine-node elements, the implementation of the RBF correction must be slightly different than for the four-node elements of [10]. Assuming an isotropic elastic material, the transverse shear strain energy for a single element is defined as follows:

$$\mathscr{W}_\gamma = 2h \int_{-1}^{+1} \int_{-1}^{+1} \left(G_1^* \, \varepsilon_{13}^2 + G_2^* \, \varepsilon_{23}^2 \right) \, J \, \mathrm{d}\xi \, \mathrm{d}\eta, \qquad (20)$$

where the corrected shear moduli are defined separately for each direction, i.e.

$$G_1^* = \left(\frac{1}{G} + \frac{l_1^2}{h^2 E} \right)^{-1}, \qquad G_2^* = \left(\frac{1}{G} + \frac{l_2^2}{h^2 E} \right)^{-1}. \qquad (21)$$

Here l_1 and l_2 are the lengths of vectors connecting opposite mid-side points. To avoid an excessive twist, the full RBF correction is applied to the value at center and only a fraction of it to the remaining part. An integrand of Eq. (20) is modified as follows:

$$G_1^* \, \varepsilon_{13}^2 \approx G_1^* \, (\bar{\varepsilon}_{13}^c)^2 + G_{1c}^* \, \left[\varepsilon_{13}^2 - (\bar{\varepsilon}_{13}^c)^2 \right], \qquad (22)$$

where

$$G_{1c}^* \doteq \left(\frac{1}{G} + a \, \frac{l_1^2}{h^2 E} \right)^{-1}, \qquad a \doteq \frac{c}{c + (1 - c) \, (l_1/l_2)^2}, \qquad (23)$$

and $c = 0.04$, as suggested in [11]. Similar formulas are used for $G_2^* \, \varepsilon_{23}^2$. For more details on our implementation of the RBF method, see [19] Sect. 13.2.3.

3. Comparing the displacements u_y of our Fig. 6b and Fig. 6 of [9] (in both figures the log-log scale is used, but actually for this scale, the differences are not clearly visible), we conclude that the elements 9-EAS11/DISP/ANS and MITC9i perform in this test slightly better than Q2-ANS/EAS. If we use the RBF correction then MITC9i performs similarly to the Q2-DSG/DSG element of [9].

5.3 Pinched Hemispherical Shell with Hole

A hemispherical shell with an 18° hole is loaded by two pairs of equal but opposite external forces P applied along the 0X and 0Y axes, see Fig. 7. Because of a double symmetry, a quarter of the hemisphere is modeled. In this test, the shell undergoes an
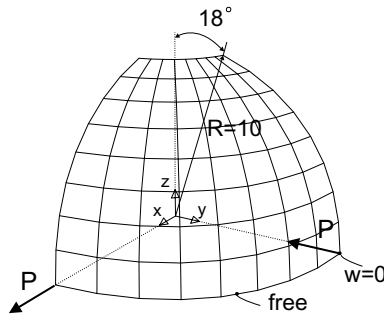

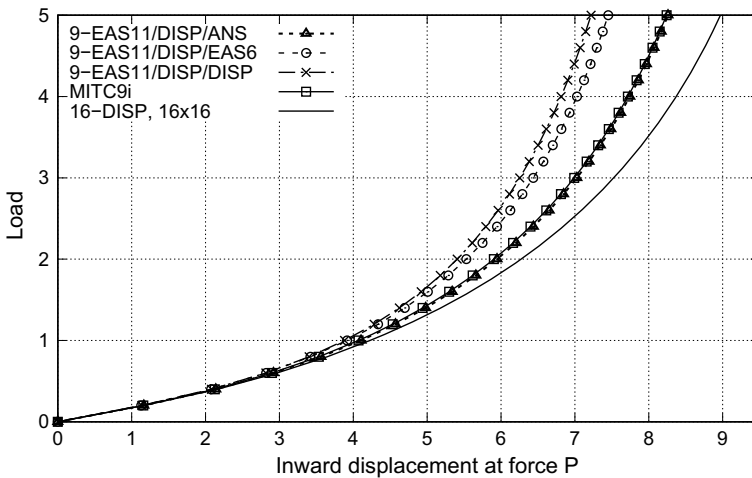**Fig. 7** Pinched hemispherical shell with hole. Geometry and load

Fig. 8 Pinched hemispherical shell with hole. Nonlinear solutions. 8×8 mesh, $\mu = G/1000$

almost inextensional deformation and, because it is very thin (thickness $h = 0.01$), the membrane locking can manifest itself strongly.

The non-linear analyses are performed using the Newton method and $\Delta P = 0.2$. The solution curves for the 8×8-element mesh are shown in Fig. 8, where the inward displacement under the force is presented.

We see that the solutions for 9-EAS11/DISP/ANS and MITC9i coincide, while for 9-EAS11/DISP/EAS6 and 9-EAS11/DISP/DISP are stiffer. For the 16×16-element mesh, the solutions for 9-EAS11/DISP/ANS and MITC9i coincide with that for the reference element 16-DISP.

6   Final Remarks

We have developed three nine-node quadrilateral shell elements with the membrane part enhanced by the EAS method; they are designated 9-EAS11 because the strain enhancement uses 11 parameters. The preliminary conclusions are as follows:

1. Using the EAS11 enhancement, the membrane patch test is passed for all types of shifts of nodes, even these for which the element's edges are curved. The modified EAS transformation rule was also implemented, but further tests are needed to draw a conclusion on its usefulness.
2. For the transverse shear part of the 9-EAS11 element, the ANS method is more accurate than the EAS6 enhancement and the unmodified strains. Accuracy of the 9-EAS11/DISP/ANS element is similar or slightly higher than of the MITC9i element, but MITC9i with the RBF correction is more accurate.
3. The Corrected Shape Functions (CSF) are not needed for the 9-EAS11 elements to pass the membrane patch test, but are beneficial for the bending patch test, like for the MITC9i element.

Generally, the preliminary results indicate that the 9-EAS11/DISP/ANS element compares very well with our MITC9i element.

References

1. Badur, J., Pietraszkiewicz, W.: On geometrically non-linear theory of elastic shells derived from pseudo-Cosserat continuum with constrained micro-rotations. In: Pietraszkiewicz, W. (ed.) Finite Rotations in Structural Mechanics, pp. 19–32. Springer, Berlin (1986)
2. Bischoff, M., Ramm, E.: Shear deformable shell elements for large strains and rotations. Int. J. Num. Meth. Eng. **40**, 4427–4449 (1997)
3. Celia, M.A., Gray, W.G.: An improved isoparametric transformation for finite element analysis. Int. J. Num. Meth. Eng. **20**, 1447–1459 (1984)
4. Huang, H-Ch.: Static and Dynamic Analyses of Plates and Shells. Springer, Berlin (1989)
5. Huang, H.C., Hinton, E.: A nine node Lagrangian Mindlin plate element with enhanced shear interpolation. Eng. Comput. **1**, 369–379 (1984)

6. Jang, J., Pinsky, P.M.: An assumed covariant strain based 9-node shell element. Int. J. Num. Meth. Eng. **24**, 2389–2411 (1987)
7. Jarzebski, P., Wisniewski, K., Taylor, R.L.: On parallelization of the loop over elements in FEAP. Comput. Mech. **56**(1), 77–86 (2015)
8. Korelc, J.: Multi-language and multi-environment generation of nonlinear finite element codes. Eng. Comput. **18**, 312–327 (2002)
9. Koschnick, F., Bischoff, G.A., Camprubi, N., Bletzinger, K.U.: The discrete strain gap method and membrane locking. Comput. Methods Appl. Mech. Eng. **194**, 2444–2463 (2005)
10. MacNeal, R.H.: A simple quadrilateral shell element. Comput. Struct. **8**(2), 175–183 (1978)
11. MacNeal, R.H.: Finite Elements: Their Design and Performance. Mechanical Engineering, vol. 89. Marcel Dekker Inc., New York (1994)
12. MacNeal, R.H., Harder, R.L.: A proposed standard set of problems to test finite element accuracy. Finite Elem. Anal. Des. **1**, 3–20 (1985)
13. Panasz, P., Wisniewski, K.: Nine-node shell elements with 6 dofs/node based on two-level approximations. Part I: theory and linear tests. Finite Elem. Anal. Des. **44**, 784–796 (2008)
14. Panasz, P., Wisniewski, K., Turska, E.: Reduction of mesh distortion effects for nine-node elements using corrected shape functions. Finite Elem. Anal. Des. **66**, 83–95 (2013)
15. Park, H.C., Lee, S.W.: A local coordinate system for assumed strain shell element formulation. Comput. Mech. **15**, 473–484 (1995)
16. Robinson, J., Blackham, S.: An evaluation of lower order membranes as contained in MSC. NASTRAN, ASA and PAFEC FEM Systems, Robinson and Associates, Dorset, England (1979)
17. Sansour, C., Kollmann, F.G.: Families of 4-node and 9-node finite elements for a finite deformation shell theory. An assessment of hybrid stress, hybrid strain and enhanced strain elements. Comput. Mech. **24**, 435–447 (2000)
18. Simo, J.C., Rifai, M.S.: A class of mixed assumed strain methods and the method of incompatible modes. Int. J. Num. Meth. Eng. **29**, 1595–1638 (1990)
19. Wisniewski, K.: Finite rotation shells. Basic Equations and Finite Elements for Reissner Kinematics. Springer, Berlin (2010)
20. Wisniewski, K., Turska, E.: Improved nine-node shell element MITC9i with reduced distortion sensitivity. Comput. Mech. **62**, 499–523 (2018)
21. Wisniewski, K., Panasz, P.: Two improvements in formulation of nine-node element MITC9. Int. J. Num. Meth. Eng. **93**, 612–634 (2013)
22. Wisniewski, K., Wagner, W., Turska, E., Gruttmann, F.: Four-node Hu-Washizu elements based on skew coordinates and contravariant assumed strain. Comput. Struct. **88**, 1278–1284 (2010)
23. Zienkiewicz, O.C., Taylor, R.L.: The finite element method. In: Basic Formulation and Linear Problems, vol. 1, 4th edn. McGraw-Hill (1989)